Atmos. Chem. Phys., 26, 16501–16519, 2026
https://doi.org/10.5194/acp-26-16501-2026
© Author(s) 2026. This work is distributed under
the Creative Commons Attribution 4.0 License.

Atmospheric Chemistry and Physics
Open Access
EGU

Measurement report: Tethered balloon observations of vertically resolved aerosol size distributions during the U.S. DOE ARM CoURAGE and BNF campaigns

Yuhang Guo[1], Chongai Kuang[2], Darielle Dexheimer[3], Peter DeCarlo[4,5], Manish Shrivastava[6], Benjamin Nault[4,7,8], Ogochukwu Enekwizu[2], Yang Wang[9], Jingbo Mao[1], Gan Luo[1], Fangqun Yu[1], and Jie Zhang[1]

[1]Atmospheric Sciences Research Center, University at Albany, State University of New York, Albany, NY 12203, USA
[2]Environmental Science and Technologies Department, Brookhaven National Laboratory, Upton, NY 11973, USA
[3]Environmental Science Division, Sandia National Laboratories, Albuquerque, NM 87123, USA
[4]Department of Environmental Health and Engineering, Johns Hopkins University, Baltimore, MD 21218, USA
[5]Department of Earth and Planetary Science, Johns Hopkins University, Baltimore, MD 21218, USA
[6]Pacific Northwest National Laboratory, Richland, WA 99354, USA
[7]Institute for Planetary Health, Johns Hopkins University, Johns Hopkins University, Baltimore, MD 21218, USA
[8]Center for Aerosol and Cloud Chemistry, Aerodyne Research, Inc., Billerica, MA 01821, USA
[9]Department of Chemical, Environmental and Materials Engineering, University of Miami, Coral Gables, FL 33146, USA

Correspondence: Fangqun Yu (fyu@albany.edu) and Jie Zhang (jzhang35@albany.edu)

Received: 13 August 2026 – Discussion started: 14 September 2026
Revised: 5 November 2026 – Accepted: 9 November 2026 – Published: 19 November 2026

Abstract. The vertical distribution of aerosol particle size is important for aerosol transport, atmospheric mixing, and surface air quality, yet vertically resolved aerosol size-distribution observations remain limited. Here, a miniature scanning electrical mobility spectrometer (mSEMS) was deployed aboard the U.S. Department of Energy Atmospheric Radiation Measurement (ARM) Tethered Balloon System (TBS) during the 2025 CoURAGE and Bankhead National Forest (BNF) campaigns. Aerosol particle number size distributions were measured from the surface to approximately 1200 m above ground level (a.g.l.) over a diameter range of 10–300 nm. A total of 63 aerosol profiles were obtained, providing one of the most comprehensive vertically resolved aerosol size-distribution datasets collected using a tethered balloon platform. Within the planetary boundary layer (PBL), observations revealed vertically homogeneous profiles associated with efficient turbulent mixing and heterogeneous profiles reflecting incomplete mixing, surface influences, or elevated particle layers. Profiles extending above the PBL further resolved distinct aerosol transitions into the lower free troposphere and nocturnal residual layer. A representative case on 27 March 2025 at BNF documented the evolution of particles associated with a regional new particle formation and growth event: particles formed during the previous day were preserved overnight within the residual layer, vertically reorganized during early-morning boundary-layer development, and subsequently remixed throughout the daytime mixed layer. These observations demonstrate strong coupling between boundary-layer evolution and aerosol vertical structure and establish an observational framework linking aerosol size distributions, residual-layer storage, and atmospheric mixing. The dataset provides valuable constraints for understanding lower-tropospheric aerosol life cycles and evaluating atmospheric chemistry and transport models.

Published by Copernicus Publications on behalf of the European Geosciences Union.

1 Introduction

Atmospheric aerosol properties often vary substantially with altitude due to the combined influences of emissions, atmospheric transport, boundary-layer evolution, aerosol formation and growth, and cloud processing (Engvall et al., 2008; Yu et al., 2016; O'Donnell et al., 2023; Wang et al., 2023; Chen et al., 2025). As a result, aerosol populations observed at the surface may not be representative of those present throughout the lower troposphere. Characterizing aerosol vertical profiles is therefore important for understanding aerosol evolution, atmospheric mixing, and the exchange of aerosol populations between surface layers, residual layers, and the free troposphere (Mei et al., 2024; Rosenfeld et al., 2014; Lin et al., 2023).

Despite decades of surface-based aerosol size distribution measurements (Kulmala et al., 2012; Nieminen et al., 2018; Ling et al., 2019; Yu et al., 2020; Jokinen et al., 2022), vertically resolved observations of aerosol particle size distributions remain relatively limited (Wang et al., 2023; Kuang, 2023). Previous studies have reported elevated aerosol layers, residual-layer particle reservoirs, and vertically separated particle growth events, suggesting that aerosol evolution frequently occurs within layers that are only weakly coupled to the surface (Chen et al., 2018; Carnerero et al., 2018; Williamson et al., 2019; Zhao et al., 2020; Lampilahti et al., 2021; Lai et al., 2022; O'Donnell et al., 2023; Wang et al., 2023; Kuang, 2023). However, routine observations of vertically resolved high resolution aerosol size distributions throughout the lower troposphere remain sparse, particularly across contrasting atmospheric environments. Tethered balloon systems (TBS) provide a unique observational platform for characterizing aerosol vertical profiles because they can repeatedly measure the lower atmosphere with high vertical resolution while carrying compact aerosol instrumentation (Ran et al., 2022; Mei et al., 2025, 2026; Fan et al., 2026). Such observations can reveal aerosol layering, boundary-layer coupling, and vertical redistribution processes that are difficult to identify using surface measurements or remote-sensing observations alone. However, high-resolution vertical observations of aerosol particle size distributions remain scarce, particularly those covering both ultrafine and accumulation-mode particles. These particle size ranges encompass the majority of aerosol number concentrations and include particles relevant to cloud condensation nuclei (CCN) (Salma et al., 2011; Pöhlker et al., 2021; Dedrick et al., 2024). The lack of observations with sufficient altitude, temporal, and particle size resolution limits our understanding of how aerosol populations evolve and interact with boundary-layer processes under different atmospheric conditions.

To address this observational gap, the Department of Energy (DOE) Atmospheric Radiation Measurement (ARM)TBS deployments (Dexheimer et al., 2026) equipped with a miniature scanning electrical mobility spectrometer (mSEMS) were conducted as part of the DOE ARM-supported Seasonal/Spatial Vertical new particle formation (NPF) Variation (SSVNV, Zhang et al., 2026a) campaign during the ARM Mobile Facility 1 Coast-Urban-Rural Atmospheric Gradient Experiment (AMF1 CoURAGE) in the Baltimore region (Davis et al., 2024) and the ARM Mobile Facility 3 deployment at Bankhead National Forest (AMF3 BNF), Alabama (Kuang et al., 2023, 2026). Figure S1 in the Supplement for the locations of CoURAGE and BNF). The SSVNV field campaign was designed to investigate vertically resolved aerosol variability, boundary-layer structure, and new particle formation (NPF) processes across contrasting atmospheric and emission environments. The resulting observations provide a unique opportunity to characterize aerosol vertical structures and particle size distributions under substantially different atmospheric, emission, and boundary-layer conditions.

The primary objectives of this study are to present this high-resolution, vertically resolved aerosol dataset and to (1) characterize recurring aerosol vertical profile regimes within the planetary boundary layer (PBL), (2) identify elevated layers of small particles and other vertically heterogeneous aerosol structures, and (3) examine how these vertical structures evolve in relation to PBL-top transitions and residual-layer processes. This study provides new observational insights into the complexity and temporal evolution of aerosol vertical distributions and highlights the importance of vertically resolved measurements for understanding aerosol–boundary-layer interactions across diverse atmospheric environments.

2 Method

2.1 Vertical aerosol size distribution measurements

A miniature scanning electrical mobility spectrometer (mSEMS; Model 9404, Brechtel Manufacturing Inc.) was deployed onboard the DOE ARM TBS to obtain vertically resolved aerosol particle number size distributions throughout the lower troposphere. The mSEMS is a compact scanning mobility particle sizer that determines aerosol size distributions based on electrical mobility classification using a miniaturized differential mobility analyser (DMA) coupled with an advanced mixing condensation particle counter (aMCPC). The DMA-based sizing module measures $18 \times 13 \times 10$ cm and weighs 1.55 kg, while the aMCPC measures $18 \times 12 \times 13$ cm and weighs 1.80 kg, resulting in a combined weight of approximately 3.35 kg, excluding additional accessories. The mSEMS sampling configuration also includes a Po-210 aerosol charge neutralizer (Model 9000), a

sample flow dryer, and a particle round-jet impactor (Model 8008; 0.5 µm cut size at a flow rate of 0.7 L min^{-1}) (Brechtel mSEMS Model 9404 Instrument Manual, 2022; Mei, 2024). The airborne mSEMS measured aerosol particle number size distributions over a nominal mobility diameter range of approximately 10–300 nm using 48 logarithmically spaced size bins, with a time resolution of 15 s for all bins. The instrument provided continuous high-time-resolution measurements suitable for resolving rapid vertical changes in ultrafine, Aitken-mode, and accumulation-mode aerosol populations within the evolving boundary layer. In this study, particles of 10–80 and 80–300 nm are referred to as the Aitken (Heintzenberg et al., 2015; Bulatovic et al., 2021) and accumulation modes, respectively; the upper limit of the latter reflects the measurement range of the mSEMS, which resolved only the lower portion of the accumulation mode. The mSEMS was integrated into the TBS payload using a lightweight conductive aerosol inlet positioned near the instrument package to minimize particle transmission losses. Routine quality-control procedures included monitoring sample and sheath flow rates, checking instrument operating status, and identifying periods of unstable instrument operation. Data collected during unstable flow conditions or launch and landing transitions were excluded from subsequent analysis.

It should be noted that variations in ambient pressure, temperature, and relative humidity during TBS vertical profiling may affect aerosol particle size distribution measurements. The mSEMS was operated at an aerosol sample flow rate of 0.3 L min^{-1} and a sheath flow rate of 2.5 L min^{-1}. To minimize the influence of hygroscopic growth, sampled aerosols were passed through an aerosol dryer (ACC-Dryer; Brechtel mSEMS Model 9404 Instrument Manual, 2022) before entering the mSEMS. The sample relative humidity was typically below 40 % (approximately 36 %), and the reported particle size distributions therefore represent nominally dry rather than ambient-RH conditions. No additional correction for hygroscopic growth was applied. The DMA inversion matrix was recalculated for each scan using the measured pressure and temperature to account for their variations during vertical profiling. In addition, sample and sheath volumetric flow rates were measured using laminar flow elements, with corrections applied for temperature-dependent changes in air viscosity. No additional offline pressure, temperature, or flow corrections were applied. A short conductive aerosol inlet was used to minimize particle transmission losses; however, no additional size-dependent inlet loss correction was applied because the transmission efficiency of the complete sampling configuration was not independently characterized. Consequently, diffusional losses may lead to an underestimation of particle number concentrations, particularly for smaller particles, and may affect the relative contributions of different aerosol size modes. These potential losses were not quantitatively evaluated in this study and warrant further investigation. To characterize the vertical variability of aerosol size distributions, each flight was divided into 80 equally spaced altitude bins, and the mean particle number size distribution under ambient conditions was calculated for each bin. The resulting distributions were displayed as altitude–diameter plots, with particle mobility diameter on a logarithmic scale. For modal diameter identification, the distributions were interpolated onto a uniform logarithmic diameter grid. Local peaks were identified using SciPy (Virtanen et al., 2020) and screened by peak height, prominence, width, and separation, retaining up to two peaks per altitude bin. Modal diameters were refined by local quadratic interpolation. Peaks in adjacent altitude bins were matched based on differences in logarithmic diameter, and only tracks spanning at least two consecutive bins were displayed. The identified modal diameter profiles were overlaid on the ambient size-distribution plots. Vertical profiles of total particle number concentrations under ambient and standard temperature and pressure (STP) conditions were also displayed for comparison. The y-axis tick intervals were standardized to 100 m across figures, while the maximum altitude was adjusted according to the altitude range of each flight. Meanwhile, elevated particle concentrations were occasionally observed in the lowest size bin near 10 nm, appearing disconnected from adjacent size bins. Given the potentially greater measurement uncertainties near the lower detection limit of the mSEMS, this bin was excluded from the contour plots to avoid overinterpretation of these isolated signals.

2.2 TBS deployments at AMF1 CoURAGE and AMF3 BNF

TBS observations were conducted at the AMF1 CoURAGE and AMF3 BNF sites during multiple intensive operating periods spanning different seasons in 2025 (Tables 1 and S1 in the Supplement, Fig. 1 as examples of TBS launches during CoURAGE and BNF). The CoURAGE deployment represented an urban–coastal environment influenced by anthropogenic emissions, marine air masses, and land–sea interactions (Davis et al., 2024), whereas the BNF deployment represented a forested southeastern U.S. environment characterized by strong biogenic emissions and frequent new particle formation (Kuang et al., 2023, 2026). Together, these deployments encompassed a broad range of atmospheric, emission, and boundary-layer conditions sampled during the 2025 field campaigns. At BNF, the TBS was operated at the main site (Fig. S1b), allowing direct comparison with collocated surface and remote-sensing measurements, including Scanning Mobility Particle Sizer (SMPS), ceilometer, and Doppler lidar observations. In contrast, during CoURAGE, the TBS launch site was located approximately 36 km from the AMF1 core site (Fig. S1c). Because of this separation, and the influence of sea–land breeze circulations and heterogeneous emissions in the region, the PBL height at the TBS launch site may differ from that at the AMF1 core site. Because the wintertime PBL was shallower and the

TBS approached or exceeded the PBL top, National Oceanic and Atmospheric Administration (NOAA) High-Resolution Rapid Refresh Model (HRRR, Blaylock et al., 2017; James et al., 2022) simulated PBL heights were examined for the two wintertime CoURAGE flights presented in the main text (22 and 24 February 2025, Sect. 3.1.2 and 3.1.3). The largest spatial differences occurred over and near the Chesapeake Bay, while PBL heights at the two sites were broadly comparable. During the summertime flights, the TBS generally remained below the PBL top, so the interpretation of these profiles is less sensitive to the exact PBL height. TBS thermodynamic measurements were not used to determine the PBL height because most flights did not reach the PBL top, and because each profile took 1.5–3 h to complete, the evolving boundary layer made it difficult to identify the PBL top from a single profile. The ceilometer-derived PBL height was therefore used at both sites to maintain a consistent approach between CoURAGE and BNF.

The TBS flight operations were coordinated with routine ARM observations and conducted under favourable meteorological conditions. The measurement periods typically lasted approximately 1–2 h (Table S1), with ascent and descent generally taking comparable amounts of time, depending on the maximum altitude and operational conditions. Aerosol size distributions measured during ascent and descent were averaged within the same altitude layers to increase the number of observations and improve statistical representativeness. However, temporal variations in aerosol concentrations and atmospheric conditions may introduce differences between ascent and descent measurements, which are not fully resolved by this averaging approach. A more detailed investigation of these differences and their underlying atmospheric processes is warranted in future studies. Measurements acquired during the ascent and descent were averaged within the same altitude layers to construct the vertical aerosol size distribution profiles used in this study. Across the CoURAGE and BNF deployments, a total of 63 successful TBS flights were completed (Table 1 summarizes the campaign statistics, while detailed flight information is provided in Table S1). Of these flights, five conducted on 22–24 February during CoURAGE were measured using the Johns Hopkins University (JHU) mSEMS, while the remaining flights were obtained using the University at Albany (UAlbany) mSEMS. The TBS flights were launched from the surface, with maximum flight altitudes ranging from 106 to 1201 m above ground level (a.g.l.), depending on flight conditions and operational constraints. Meanwhile, according to TBS operational requirements, the balloon was required to remain at least 152 m (500 ft) below the cloud base, thereby avoiding direct cloud interception and minimizing potential cloud-related sampling artifacts. Most flights remained entirely within the PBL, whereas seven flights extended above the PBL into either the residual layer (5 flights) or the lower free troposphere (2 flights). The resulting dataset captures a broad range of boundary-layer conditions, including well-mixed daytime PBLs, shallow nocturnal boundary layers, residual-layer environments, and periods characterized by enhanced ultrafine particle concentrations. To better represent the diurnal evolution of the PBL and associated aerosol processes, all times reported in this study are given in local time (LT), unless otherwise specified.

3 Results

The TBS-mounted mSEMS observations revealed several recurring aerosol vertical profiles associated with different stages of boundary-layer evolution during the CoURAGE and BNF deployments in 2025. Within the planetary boundary layer, aerosol profiles ranged from vertically homogeneous structures indicative of efficient turbulent mixing to vertically heterogeneous structures reflecting incomplete mixing and localized aerosol processing (Sect. 3.1). Profiles extending above the PBL further captured distinct aerosol transitions into the lower free troposphere or the nocturnal residual layer (Sect. 3.2). Case studies demonstrated that particles formed during regional growth events can remain stored within nocturnal residual layers overnight and subsequently undergo vertical redistribution as the daytime boundary layer redevelops (Sect. 3.3). Together, these observations illustrate how vertically resolved aerosol size distributions provide direct insight into aerosol transport, mixing, and atmospheric evolution that cannot be inferred from surface observations or boundary-layer height alone.

3.1 Aerosol profiles within the PBL

Aerosol profiles within the PBL exhibited a wide range of vertical variability during the CoURAGE and BNF deployments. To characterize aerosol variability associated with mixing processes within the PBL, measurements below the ceilometer-derived PBL height were examined for all TBS profiles, regardless of whether the flights remained entirely within the PBL or extended above the PBL top. Based on the degree of vertical variability in aerosol number size distributions, the within-PBL segments of the profiles were classified into two primary categories: Type I, characterized by vertically homogeneous aerosol structures, and Type II, characterized by vertically heterogeneous aerosol structures. Type I profiles were further divided into single accumulation-mode (“Type I.A”) and bimodal profiles (“Type I.B”), whereas Type II profiles were separated into surface-influenced profiles (“Type II.A”) and upper-PBL aerosol-enriched profiles (“Type II.B”) according to the location of the dominant aerosol enhancement. The transitions observed above the PBL top are discussed separately in Sect. 3.2.

3.1.1 Vertically homogeneous aerosol profiles (“Type I”)

Vertically homogeneous aerosol structures were the dominant profile type observed during both the CoURAGE and

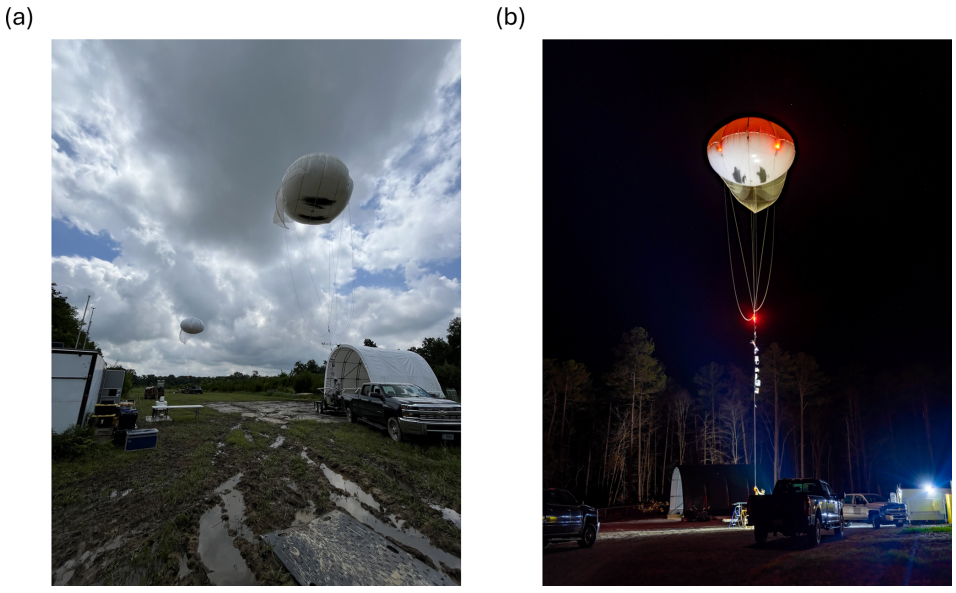

Figure 1. DOE ARM TBS deployment with mSEMS at **(a)** AMF1-CoURAGE and **(b)** AMF3-BNF in 2025

Table 1. Summary of TBS intensive observation periods (IOPs) and aerosol profile classifications during the CoURAGE and BNF campaigns in 2025.

Campaigns	IOP	Time period dd/mm–dd/mm	Season	Flights	Number of aerosol profile type Total (M/A/N)				Cross PBL Total (M/A/N)
					I.A	I.B	II.A	II.B	
CoURAGE	#1	13/02–24/02	Late winter	6	1 (0/1/0)	1 (0/1/0)	3 (1/2/0)	1 (0/1/0)	2 (2/0/0)
	#2	15/07–28/07	Summer	19	8 (3/5/0)	8 (2/6/0)	2 (1/1/0)	1 (1/0/0)	0 (0/0/0)
BNF	#3	27/03–26/04	Spring	15	10 (2/7/1)	0 (0/0/0)	3 (0/1/2)	2 (0/0/2)	5 (1/0/4)
	#4	29/05–15/06	Early Summer	15	8 (3/3/2)	6 (2/4/0)	0 (0/0/0)	1 (0/0/1)	0 (0/0/0)
	#5	09/08–23/08	Summer	8	3 (0/2/1)	5 (1/4/0)	0 (0/0/0)	0 (0/0/0)	0 (0/0/0)
Total				63	30 (8/18/4)	20 (5/15/0)	8 (2/4/2)	5 (1/1/3)	7 (3/0/4)

Note: M, A, and N denote Morning (05:00–11:59 LT), Afternoon (12:00–18:59 LT), and Night (19:00–04:59 LT) flight numbers, respectively. Numbers in parentheses indicate the corresponding flight counts (M/A/N). Type I.A refers to vertically homogeneous profiles with a single accumulation mode (Sect. 3.1.1); Type I.B refers to vertically homogeneous bimodal profiles (Sect. 3.1.1); Type II.A refers to vertically heterogeneous, surface-influenced profiles (Sect. 3.1.2); and Type II.B refers to vertically heterogeneous profiles with aerosol enrichment in the upper PBL (Sect. 3.1.2). Cross PBL indicates flights that crossed the planetary boundary layer (PBL) top and is reported separately from the four aerosol profile types.

BNF deployments, accounting for 50 of the 63 TBS measurements (Table 1), with representative examples shown in Fig. 2. Most TBS measurements (54 of 63, approximately 86 %) were conducted during daytime hours, with a substantial fraction (38 of 63, approximately 60 %) occurring in the afternoon. This sampling bias toward afternoon conditions, when the planetary boundary layer (PBL) is often well developed and vertically mixed, may have contributed to the predominance of Type I aerosol profiles. Future TBS deployments will place greater emphasis on morning measurements, particularly during the transition from the nocturnal stable boundary layer to the developing convective boundary layer, to better characterize the diurnal evolution of aerosol vertical structures.

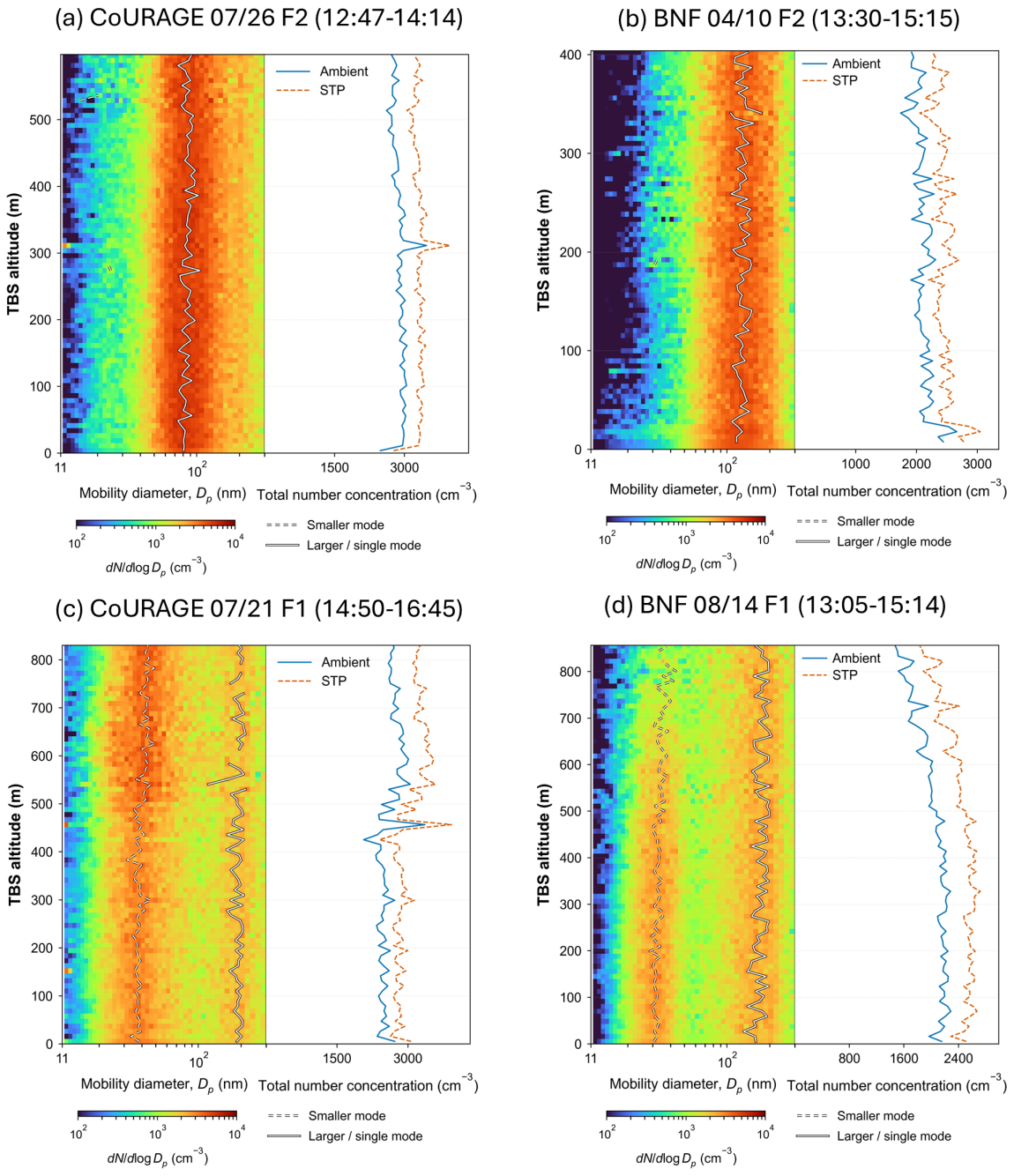

Figure 2. Aerosol vertical size distribution observed by TBS mSEMS during **(a)** CoURAGE 26 July 2025 Flight 1 between 10:40 and 12:03 LT, **(b)** BNF 10 April 2025 Flight 2 between 13:30 and 15:15 LT, **(c)** CoURAGE 21 July 2025 Flight 1 between 14:50 and 16:30 LT, and **(d)** BNF 14 August 2025 Flight 1 between 13:05 and 15:14 LT. The color shading represents particle number size distributions under ambient conditions. Solid and dashed gray lines indicate the identified larger (or single) and smaller particle modes, respectively. The right-hand panels show vertical profiles of total particle number concentrations under ambient conditions (blue solid lines) and normalized to standard temperature and pressure (STP; orange dashed lines).

In these profiles, aerosol size distributions remained nearly constant with altitude, indicating efficient vertical mixing and strong coupling between surface and elevated aerosol populations (Zhao et al., 2025; Canales et al., 2025). Most homogeneous profiles (30 of 50) were characterized by a single accumulation-mode peak centered at approximately 80–150 nm and were classified as "Type I.A" (single accumulation-mode profiles, Figs. 2a, b, and S3). All Type I.A profiles were obtained during late morning, afternoon, or evening, when the PBL was well developed. Un-

der these conditions, the maximum TBS sampling altitude remained below the ceilometer-derived PBL height, and the measurements therefore captured only the well-mixed portion of the boundary layer. The accumulation mode dominated the aerosol population throughout the sampled vertical range with little variation in modal diameter or relative contribution, consistent with efficient turbulent mixing that minimized vertical gradients in aerosol size distributions. Type I.A profiles were observed during both winter, spring and summer deployments for both CoURAGE and BNF, indicating that this vertically homogeneous single accumulation-mode profile is not restricted to a particular season but represents a common feature of well-mixed boundary layers under a range of atmospheric conditions.

The remaining 20 vertically homogeneous profiles exhibited persistent bimodal aerosol size distributions and were classified as "Type I.B". These profiles were characterized by a distinct Aitken-mode population centered at approximately 20–50 nm together with an accumulation-mode peak near 100–200 nm (Figs. 2c, d, and S3). Similar to Type I.A, both modes showed little variation with altitude throughout the sampled PBL, indicating that the two aerosol populations were well mixed within the boundary layer rather than being confined to either the surface layer or a narrow elevated layer.

A pronounced seasonal and diurnal preference was evident for Type I.B profiles. Nineteen of the twenty cases occurred during the late-spring and summer deployments, while fourteen were observed during afternoon flights and most of the remaining cases occurred during late morning (approximately 11:00–12:00 LT). Thus, bimodal profiles were observed almost exclusively from late morning through the afternoon, when photochemical activity and boundary-layer mixing were generally strongest (Lee et al., 2009; Seinfeld and Pandis, 2016; Fischer et al., 2019). The occurrence of Type I.B profiles during both the CoURAGE and BNF deployments indicates that this behavior was not unique to a single site despite the contrasting atmospheric environments of the two campaigns. The CoURAGE deployment sampled a coastal agricultural environment influenced by marine and anthropogenic air masses (Davis et al., 2024), whereas the BNF deployment represented a forested southeastern environment with strong biogenic influences (Kuang et al., 2023, 2026). The presence of similar vertically homogeneous bimodal structures at both locations suggests that this profile type represents a recurring feature of summertime boundary-layer aerosol evolution across different environmental settings.

Concurrent surface SMPS observations at the BNF site provided valuable temporal context for interpreting the TBS observations. The surface measurements showed that a Aitken mode centered at approximately 20–50 nm repeatedly emerged from late morning through the afternoon and frequently persisted into the evening on multiple days, as illustrated by the weekly SMPS measurements covering the BNF TBS deployments on 29 May, 14 August, and 16 August (Fig. 3). The repeated daytime appearance of this mode indicates that the bimodal aerosol structure was associated with systematic daytime atmospheric processing rather than isolated events. Together, the complementary surface and TBS observations suggest that, by the time of the balloon measurements, the Aitken-mode particles had become broadly distributed throughout the daytime mixed layer, producing vertically homogeneous bimodal aerosol profiles.

Although the observed bimodal profiles shared similar vertical characteristics, the available observations suggest that the processes responsible for the Aitken mode likely varied among individual cases. For many summertime cases, the repeated afternoon appearance of the 20–50 nm mode could be consistent with daytime new particle formation followed by condensational growth into the Aitken-size range (Seinfeld and Pandis, 2016; Young and Keeler, 2007; Carlton et al., 2018). Pronounced classical banana-shaped growth was not evident in many events; however, the recurring daytime emergence of the Aitken mode suggests that new particle formation and growth may nevertheless have occurred under relatively high background aerosol loadings, where the earliest stages of growth were either not resolved or partially obscured by efficient particle sinks (June et al., 2026). Consequently, the observed Aitken mode likely represented a relatively mature ultrafine-particle population rather than freshly nucleated particles. Given that this study is intended primarily as an observational characterization of aerosol vertical structures, distinguishing among these potential formation pathways is beyond the scope of the present work. Future studies integrating the TBS observations with chemical transport model simulations and additional process analyses will provide a more comprehensive assessment of the mechanisms responsible for the observed Type I.B profiles.

Not all Type I.B profiles, however, appeared to evolve through the same pathway. In contrast to profiles such as that on 14 August at BNF (Fig. 2d), in which the Aitken mode was most evident in the lower boundary layer and likely originated from near-surface formation and growth, the 16 August case suggests a pathway in which particles were introduced from aloft. During the 16 August 2025 BNF flights, the evolution of the Aitken mode was captured simultaneously by the TBS (Fig. 4a and b), continuous surface SMPS measurements (Fig. 3b), and Doppler lidar observations (Fig. 4c). During the TBS ascent (Fig. 4a), the 20–50 nm particle population was largely absent in the lowest portion of the boundary layer, whereas the same mode became evident near the surface during the subsequent descent approximately 30 min later (Fig. 4b). The integrated Aitken-mode particle number concentrations (10–80 nm) further support this evolution. During the ascent, ambient Aitken-mode number concentrations increased with altitude, reaching approximately 800–900 cm^{-3} in the upper boundary layer, compared with approximately 400 cm^{-3} near the surface. During the descent, ambient near-surface concentrations increased to approximately 800–1000 cm^{-3}, comparable to those observed aloft

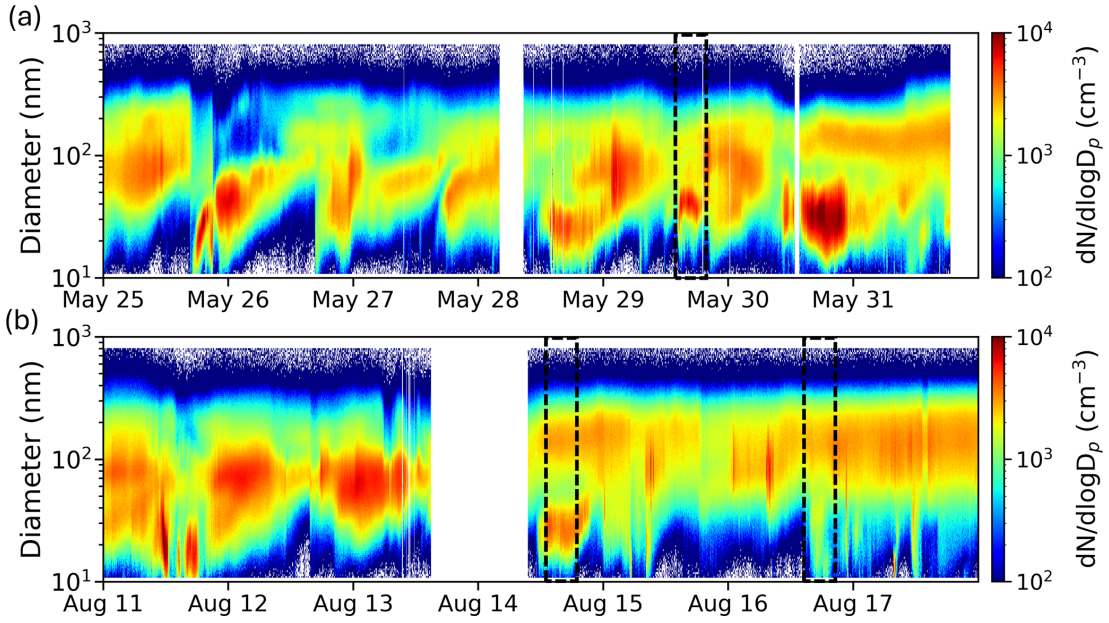

Figure 3. Time series of surface aerosol particle number size distributions measured at BNF during 25–31 May and 11–17 August 2025 (LT, UTC−5). The dashed black boxes indicate the TBS deployment periods.

during the ascent, while the vertical concentration gradient became substantially weaker. This redistribution is consistent with the downward mixing of Aitken-mode particles from the upper boundary layer. Concurrently, the surface SMPS recorded the appearance of the Aitken mode at approximately 16:00 LT (Fig. 3b), closely matching the timing of the TBS observations. Doppler lidar measurements during the same period indicated active vertical motions within PBL, providing additional evidence for enhanced turbulent exchange between the upper boundary layer and the mixed layer. Doppler lidar wind profiles also showed relatively weak horizontal winds (Fig. S4), with wind speeds predominantly below 5 m s^{-1} within the lowest 1 km. Although horizontal advection cannot be entirely excluded, these observations suggest that strong horizontal transport was unlikely to be the dominant driver of the observed changes in aerosol vertical distributions. Taken together, these independent observations are consistent with rapid downward mixing or entrainment of an aerosol population from aloft, followed by efficient turbulent redistribution throughout the daytime boundary layer. The observed evolution also suggests a possible link between the upper-PBL aerosol-enriched profiles (Type II.B in following section) and the vertically homogeneous bimodal profiles (Type I.B). Under favorable mixing conditions, the elevated Aitken-mode particle population may be mixed downward and redistributed throughout the boundary layer, providing one plausible pathway for the development of Type I.B profiles. Further observations will be required to assess the prevalence of this evolutionary pathway.

Overall, these observations indicate that Type I.B represents a recurring summertime aerosol profile rather than a unique formation mechanism. While many cases are consistent with daytime photochemical production and subsequent particle growth, others appear to be more strongly influenced by boundary-layer dynamics, including entrainment and rapid turbulent redistribution. Regardless of the specific formation pathway, the common characteristic of all Type I.B profiles is the vertically homogeneous coexistence of Aitken- and accumulation-mode particles throughout the sampled boundary layer.

3.1.2 Vertically heterogeneous aerosol structures ("Type II")

Although vertically homogeneous profiles were the dominant aerosol type observed during the TBS deployments, a substantial fraction of the measurements (13 of the 63 profiles) exhibited pronounced vertical heterogeneity in aerosol size distributions within the sampled PBL. In these profiles, aerosol populations varied considerably with altitude, indicating incomplete vertical mixing and reflecting the combined influences of boundary-layer dynamics, aerosol processing, and localized transport. The heterogeneous profiles comprised two distinct patterns, with (1) eight profiles exhibiting pronounced surface influence and were classified as Type II.A (Table S1 and Fig. 5a, b) and (2) five profiles exhibiting upper-PBL aerosol-enriched layers and were classified as Type II.B (Table S1 and Fig. 5c, d).

The Type II.A profiles were characterized by enhanced concentrations of Aitken-mode particles and broader aerosol

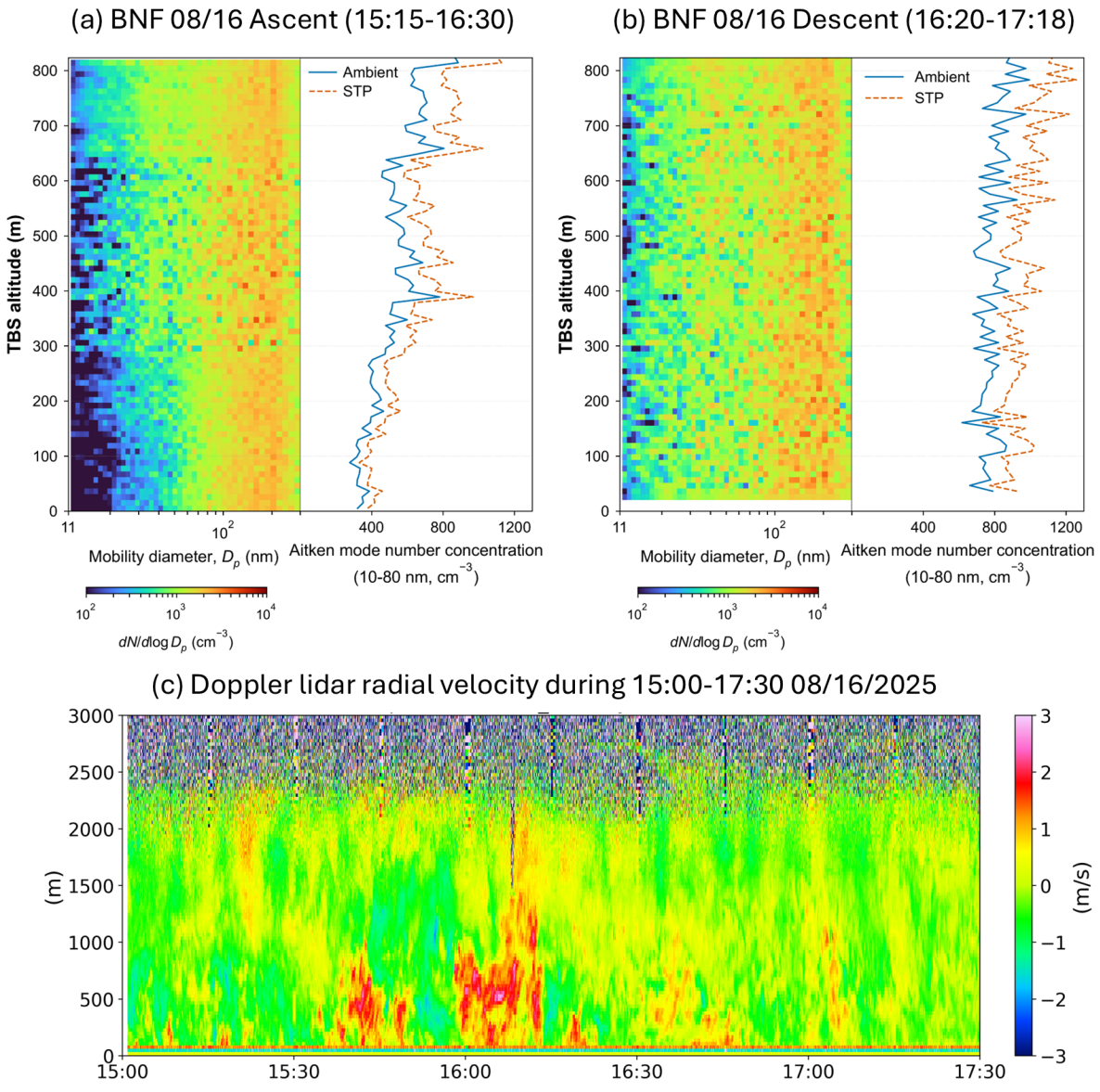

Figure 4. Vertical distributions of aerosol particle size distributions and Aitken-mode particle number concentrations measured by the TBS-mounted mSEMS during the BNF campaign on 16 August 2025: **(a)** ascent (15:15–16:30 LT) and **(b)** descent (16:30–17:18 LT). The color contours represent particle number size distributions, while the blue solid and orange dashed lines indicate integrated Aitken-mode particle number concentrations (10–80 nm) under ambient and standard temperature and pressure (STP) conditions, respectively. **(c)** Doppler lidar radial velocity during the TBS deployments.

size distributions within the lowest several hundred meters of the boundary layer (Figs. 5a, b, and S6). With increasing altitude, the contribution of smaller particles gradually decreased, and the aerosol population transitioned toward a relatively uniform accumulation-mode distribution centered at approximately 80–150 nm. Unlike the upper-PBL aerosol-enriched profiles described in the following section, Type II.A profiles did not contain distinct elevated aerosol layers. Instead, aerosol properties changed gradually with altitude, indicating a progressive weakening of surface influences away from the ground rather than an abrupt transition between separate aerosol populations. The enhanced abundance of Aitken-mode particles near the surface is consistent with stronger impacts of local emissions and near-surface aerosol processing, whereas aerosol populations aloft appeared more representative of the regionally mixed boundary layer. These observations suggest that local surface sources can remain evident within the lower PBL despite substantial daytime turbulent mixing. One notable example of a Type II.A profile was observed under nocturnal boundary-layer conditions, when a shallow stable PBL confined locally influenced aerosol populations within the lowest few hundred

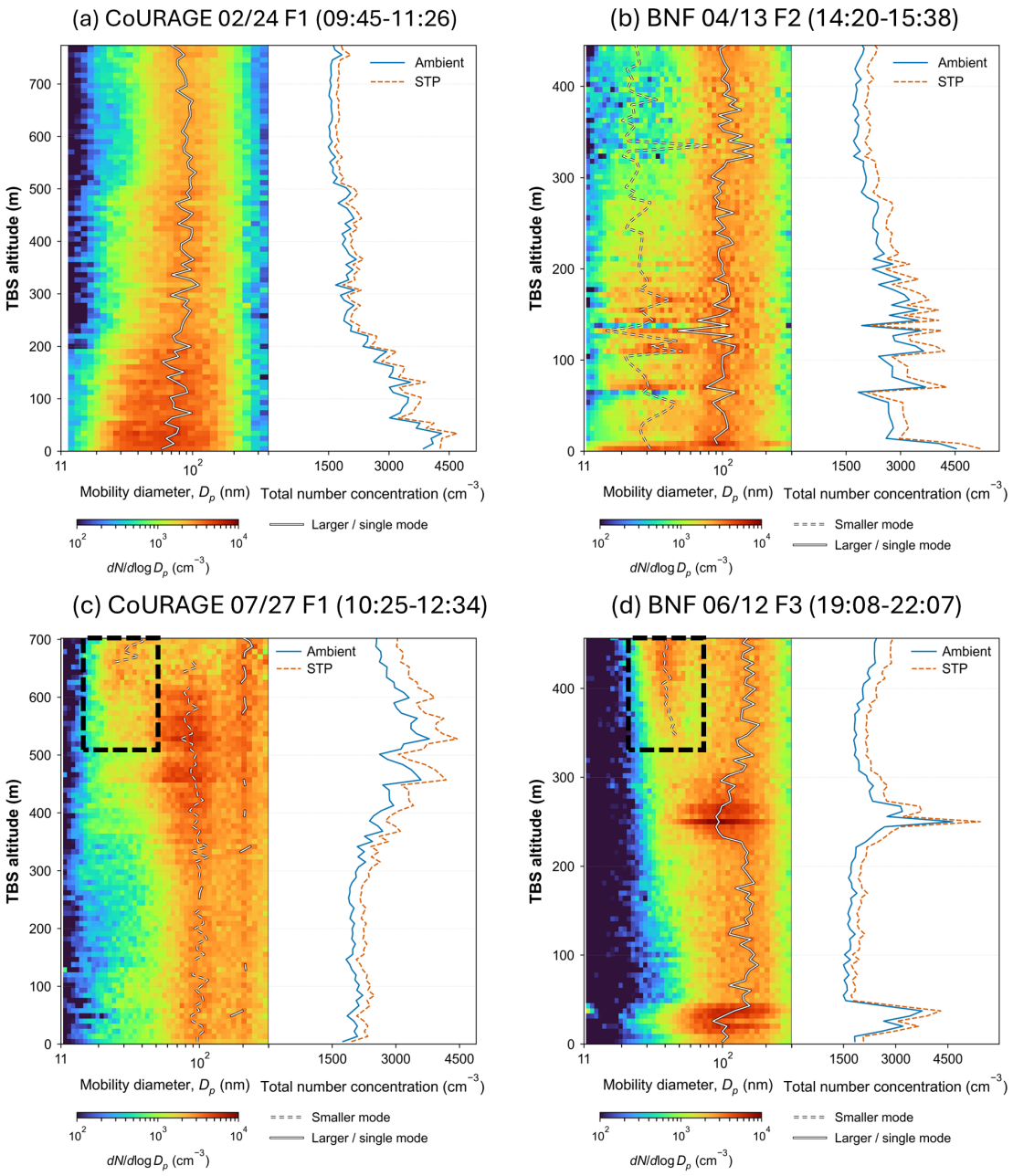

Figure 5. Aerosol vertical size distribution observed by TBS mSEMS during **(a)** CoURAGE 24 February 2025 Flight 1 between 09:45 and 11:26 LT, **(b)** BNF 13 April 2025 Flight 2 between 14:20 and 15:38 LT, **(c)** CoURAGE 27 July 2025 Flight 1 between 10:25 and 12:34 LT, and **(d)** BNF 12 June 2025 Flight 1 between 19:08 and 22:07 LT. The color shading represents particle number size distributions under ambient conditions. Solid and dashed gray lines indicate the identified larger (or single) and smaller particle modes, respectively. The right-hand panels show vertical profiles of total particle number concentrations under ambient conditions (blue solid lines) and normalized to standard temperature and pressure (STP; orange dashed lines). The black dashed boxes in panels **(c)** and **(d)** highlight the Aitken-mode aerosol enrichment in the upper planetary boundary layer (PBL).

meters while the overlying residual layer remained comparatively well mixed. This case illustrates how a shallow nighttime boundary layer can preserve strong vertical gradients in aerosol size distributions despite relatively weak changes in total particle concentrations. A more detailed analysis of this event is presented in Sect. 3.3 for "Case Study".

In contrast, the Type II.B profiles were characterized by enhanced concentrations of Aitken-mode particles confined to the upper portion of the boundary layer (Figs. 5c, d,

and S6), while the surrounding atmosphere remained dominated by broader accumulation-mode populations centered at 80–150 nm. Representative examples were observed during both the CoURAGE (27 July) and BNF (12 June) deployments, and aerosol layers enriched in particles between 20 and 80 nm were identified within the upper PBL (black dash box in Fig. 5c, d), typically between 300 and 700 m above ground level. During the 27 July CoURAGE flight (Fig. 5c), the elevated concentrations of 20–60 nm particles occurred between 450 and 700 m. Meanwhile, a vertically uniform accumulation mode was also present throughout the boundary layer during this flight, which may represent a well-mixed, aged regional background aerosol population. During the 12 June BNF flight (Fig. 5d), a distinct layer enriched in 30–80 nm particles was observed between approximately 300 and 450 m. In addition, a relatively concentrated accumulation-mode aerosol layer centered near 100–150 nm was present at 230–260 m, indicating that multiple vertically stratified aerosol populations coexisted within the boundary layer during this flight. In each case, the enhanced small-particle population was vertically confined and clearly distinguishable from the aerosol populations both above and below it.

Looking back at the 16 August 2025 case (Type I.B, Sect. 3.1.1), this observation further suggests a possible link between the upper-PBL aerosol-enriched profiles (Type II.B) and the vertically homogeneous bimodal profiles (Type I.B). During this event, an Aitken-mode population initially confined to the upper portion of the boundary layer was subsequently observed throughout the lower boundary layer within approximately 30 min, coincident with enhanced turbulent mixing inferred from Doppler lidar observations (Fig. 4c). This evolution suggests that, under favorable mixing conditions, upper-PBL aerosol-enriched profiles may evolve into vertically homogeneous bimodal profiles through entrainment and turbulent redistribution. Although additional observations are required to determine how frequently this pathway occurs, the present observations demonstrate that such an evolution is physically plausible. The formation of these upper-PBL aerosol-enriched profiles likely involves multiple atmospheric processes. Possible mechanisms include particle formation and growth within the upper PBL, entrainment associated with boundary-layer growth, residual-layer storage, downward transport of aerosol populations from above the PBL, and subsequent turbulent redistribution within the boundary layer. The observations presented in Sect. 3.2 and 3.3 further demonstrate that Aitken-mode particle populations can also be present within the residual layer and lower free troposphere, suggesting these regions may serve as temporary reservoirs for upper-PBL aerosol populations. The vertically confined Aitken-mode particle populations observed in these profiles suggest that aerosol processing can occur within the upper PBL independently of near-surface conditions.

3.2 Aerosol transitions across the PBL top

Although most TBS flights remained entirely within the PBL, seven flights extended above the ceilometer-derived PBL height, providing direct observations of aerosol vertical structures across the PBL top. These measurements captured transitions from the daytime mixed layer into the lower free troposphere or from the nocturnal boundary layer into the overlying residual layer. Compared with the relatively homogeneous aerosol structures frequently observed within the PBL, the profiles crossing the PBL top exhibited more pronounced changes in aerosol size distributions, reflecting the contrasting aerosol populations on either side of the boundary-layer interface. Because the physical characteristics of the lower free troposphere and the nocturnal residual layer differ substantially, these two transition types are discussed separately below.

3.2.1 Transitions from the daytime PBL to the lower free troposphere

Two morning TBS flights extended above the planetary boundary layer (PBL) into the lower free troposphere, providing direct observations of aerosol vertical transitions across the daytime PBL top (Fig. 6a and b). These transitions were captured during the morning, when the daytime PBL was still relatively shallow and the maximum TBS sampling altitude was sufficient to extend above the PBL top. In both cases, aerosol size distributions changed abruptly upon crossing the ceilometer-derived PBL height (red dashed lines in Fig. 6; Table S1). In contrast to the relatively homogeneous aerosol profiles observed within the well-mixed boundary layer below the transition, the overlying lower free troposphere exhibited substantially different aerosol profiles, indicating a sharp transition in aerosol characteristics rather than a gradual decrease in particle concentrations with altitude.

Despite occurring during different field campaigns, the 22 February CoURAGE and 13 April BNF flights exhibited remarkably similar aerosol transition profiles. In both cases, aerosol size distributions remained nearly uniform throughout the daytime mixed layer before changing abruptly near the ceilometer-derived PBL height (approximately 750 m on 22 February CoURAGE flight and 850 m on 13 April BNF flight). Above the transition, accumulation-mode particles decreased substantially whereas smaller particles remained detectable, producing aerosol profiles distinctly different from those observed within the underlying mixed layer.

Although aerosol number concentrations generally decreased above the transition altitude, aerosol particles remained present within the lower free troposphere. In both cases, accumulation-mode particles centered at approximately 80–150 nm were substantially depleted above the PBL top, whereas Aitken-mode particles at around 20–30 nm remained detectable, resulting in a relative enhance-

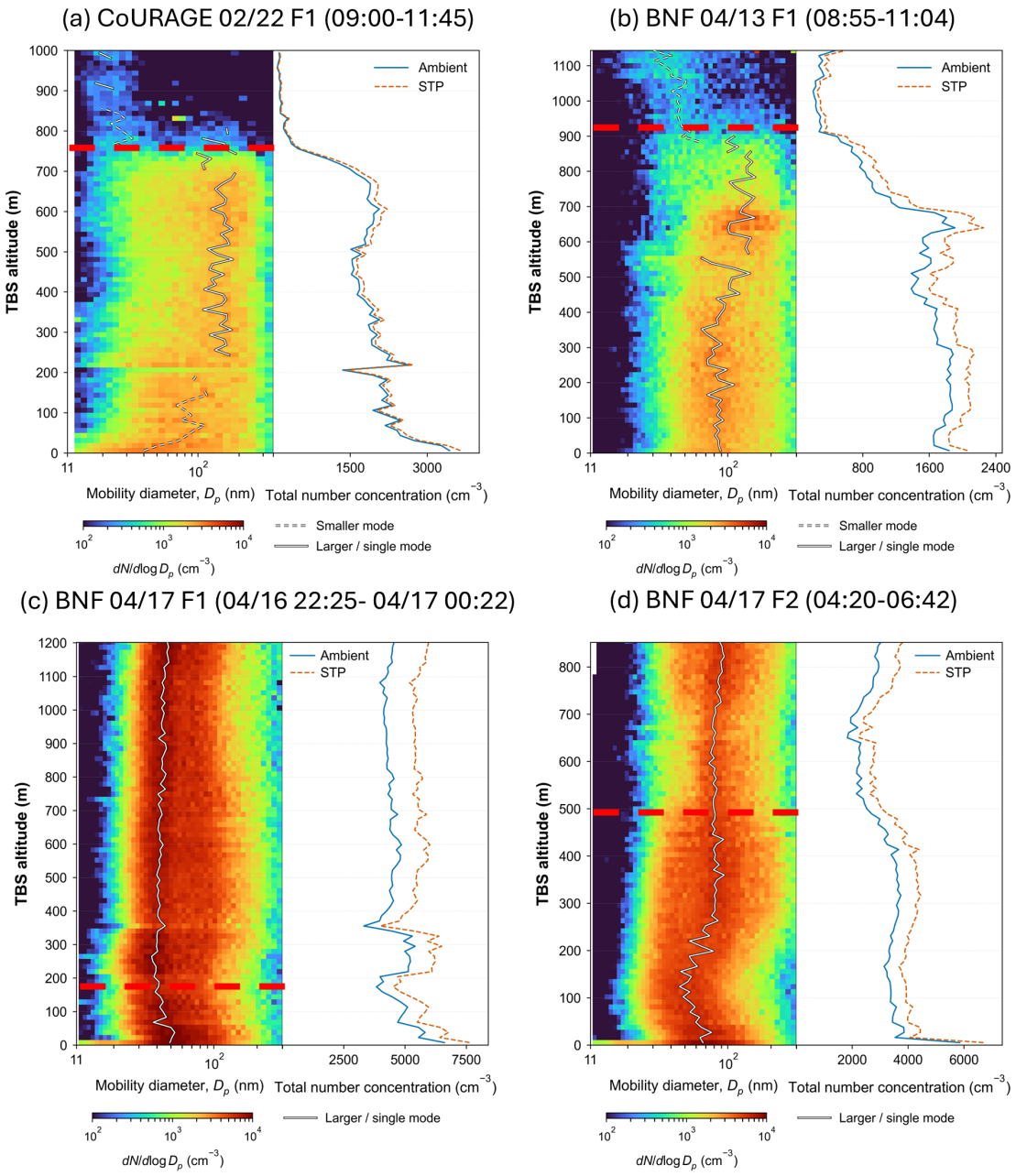

Figure 6. Aerosol vertical size distribution observed by TBS mSEMS during CoURAGE **(a)** 22 February 2025 Flight 1 between 09:00 and 11:45 LT, **(b)** BNF 13 April 2025 Flight 1 between 08:55 and 11:04 LT, **(c)** BNF 17 April 2025 Flight 1 between 22:25 and 00:22 LT, and **(d)** BNF 17 April 2025 Flight 2 between 04:20 and 06:42 LT. The color shading represents particle number size distributions under ambient conditions. Solid and dashed gray lines indicate the identified larger (or single) and smaller particle modes, respectively. The right-hand panels show vertical profiles of total particle number concentrations under ambient conditions (blue solid lines) and normalized to standard temperature and pressure (STP; orange dashed lines). The red dashed lines indicated the ceilometer-derived boundary layer heights of each flight.

ment of smaller particle populations aloft. Several processes may contribute to this contrast. Accumulation-mode particles associated with surface emissions and atmospheric aging may be preferentially confined within the PBL, with limited exchange across the capping inversion. In addition, accumulation-mode particles may be more readily activated as cloud condensation nuclei and subsequently removed through cloud processing and precipitation, whereas smaller Aitken-mode particles are generally less readily activated (Seinfeld and Pandis, 2016). The reduced abundance

of accumulation-mode particles above the PBL may also result in lower condensation and coagulation sinks, potentially favoring the survival of small particles and new particle formation in the lower free troposphere, as suggested by previous studies (Williamson et al., 2019; Zhao et al., 2020). The Aitken-mode particles observed aloft may therefore have originated from earlier particle formation and growth, transport from other regions or altitudes, or residual particle populations from previous events. However, the present observations lack the aerosol composition, precursor measurements, and air-mass history needed to distinguish among these possibilities. Future studies combining TBS profiles with back-trajectory analyses and chemical measurements could help clarify their origins.

Consequently, aerosol size distributions above the PBL differed markedly from those within the underlying mixed layer, reflecting a pronounced reduction in accumulation-mode particles while retaining a detectable Aitken-mode population. Similar observations of persistent ultrafine particles in the lower free troposphere have been reported previously (Chen et al., 2018; Lampilahti et al., 2021; Wang et al., 2023; O'Donnell et al., 2023; Liu et al., 2024; Shan et al., 2025; Zhang et al., 2026). These observations demonstrate that the lower free troposphere can contain aerosol profiles distinct from those within the underlying daytime mixed layer, highlighting the importance of vertically resolved aerosol size-distribution measurements for characterizing aerosol stratification across the PBL top.

3.2.2 Transitions from the nocturnal PBL to the residual layer

Unlike the daytime transitions into the lower free troposphere, four nighttime TBS flights extended above the shallow nocturnal planetary boundary layer into the overlying residual layer (27 March BNF F1, F2 and 17 April BNF F1, F2), providing direct observations of aerosol vertical transitions across the nocturnal PBL top (Figs. 6c and 6d for the representative examples from the 17 April BNF flights, with 27 March BNF flights discussed in Sect. 3.3). These transitions were captured after sunset or before sunrise, when the stable nocturnal boundary layer was substantially shallower than the daytime mixed layer, allowing the TBS to simultaneously sample the near-surface stable layer and the overlying residual layer. In contrast to the daytime PBL-top transitions, aerosol size distributions generally changed more gradually across the nocturnal PBL top, reflecting the greater similarity between aerosol populations in the residual layer and those remaining within the underlying stable boundary layer.

During the late-evening 17 April BNF flight (22:25–00:22 LT; Fig. 6c), the ceilometer-derived nocturnal PBL was only about 100 m deep, whereas the TBS sampled aerosol populations throughout the overlying residual layer to an altitude of 1200 m. Aerosol size distributions remained broadly similar above the shallow nocturnal boundary layer, indicating that a substantial fraction of the aerosol population resided within the residual layer rather than being confined to the stable surface layer. During the subsequent early-morning flight (04:20–06:42 LT; Fig. 6d), the nocturnal PBL had deepened to 450 m. Overall, aerosol populations aloft remained broadly consistent with those observed during the preceding late-evening flight, although noticeable changes in aerosol size distributions were evident near the residual-layer interface, suggesting the presence of vertical stratification within the residual layer. These aerosol transitions around 500–600 m coincided with enhanced wind shear near the nocturnal PBL top (Fig. S7), consistent with the dynamical separation between the shallow stable boundary layer and the overlying residual layer.

The overall similarity between the late-evening and early-morning observations indicates that the aerosol populations within the residual layer were largely preserved overnight, with no evidence of substantial changes in the overall aerosol size distributions during the intervening period. Compared with the daytime lower free troposphere, the residual layer retained aerosol populations that were much more similar to those within the underlying daytime boundary layer, consistent with the residual layer acting as a reservoir of aerosols that had been mixed throughout the daytime PBL prior to nocturnal stabilization. Representative case studies illustrating the evolution of aerosol populations within the nocturnal residual layer are presented in Sect. 3.3. In particular, the 27 March 2025 BNF flight observations document the evolution from daytime new particle formation to the subsequent preservation of the resulting aerosol population within the nocturnal residual layer, providing one of the clearest examples of the aerosol life cycle captured during the TBS deployments

3.3 Case study: aerosol evolution from daytime new particle formation to nocturnal residual-layer stratification

To investigate how particles formed during NPF events are redistributed vertically during boundary-layer evolution, we selected the TBS observations on 27 March 2025 at BNF as a representative case. Surface SMPS measurements (Fig. 7a) showed repeated NPF and subsequent particle growth between 22 and 28 March 2025, with elevated concentrations frequently persisting into the following day. The observations on 27 March captured the transition from a shallow nocturnal boundary layer to a fully developed daytime mixed layer (Fig. 7b), allowing the vertical evolution of particles associated with the previous day's growth event to be examined.

During Flight 1 (26 March, 21:22–23:15 LT; Fig. 7c), aerosol size distributions were nearly identical throughout the sampled profile from the surface to 700 m. Only a subtle reduction in particles smaller than 30 nm was observed within a narrow layer near the top of the shallow nocturnal boundary layer (approximately 70–100 m), while par-

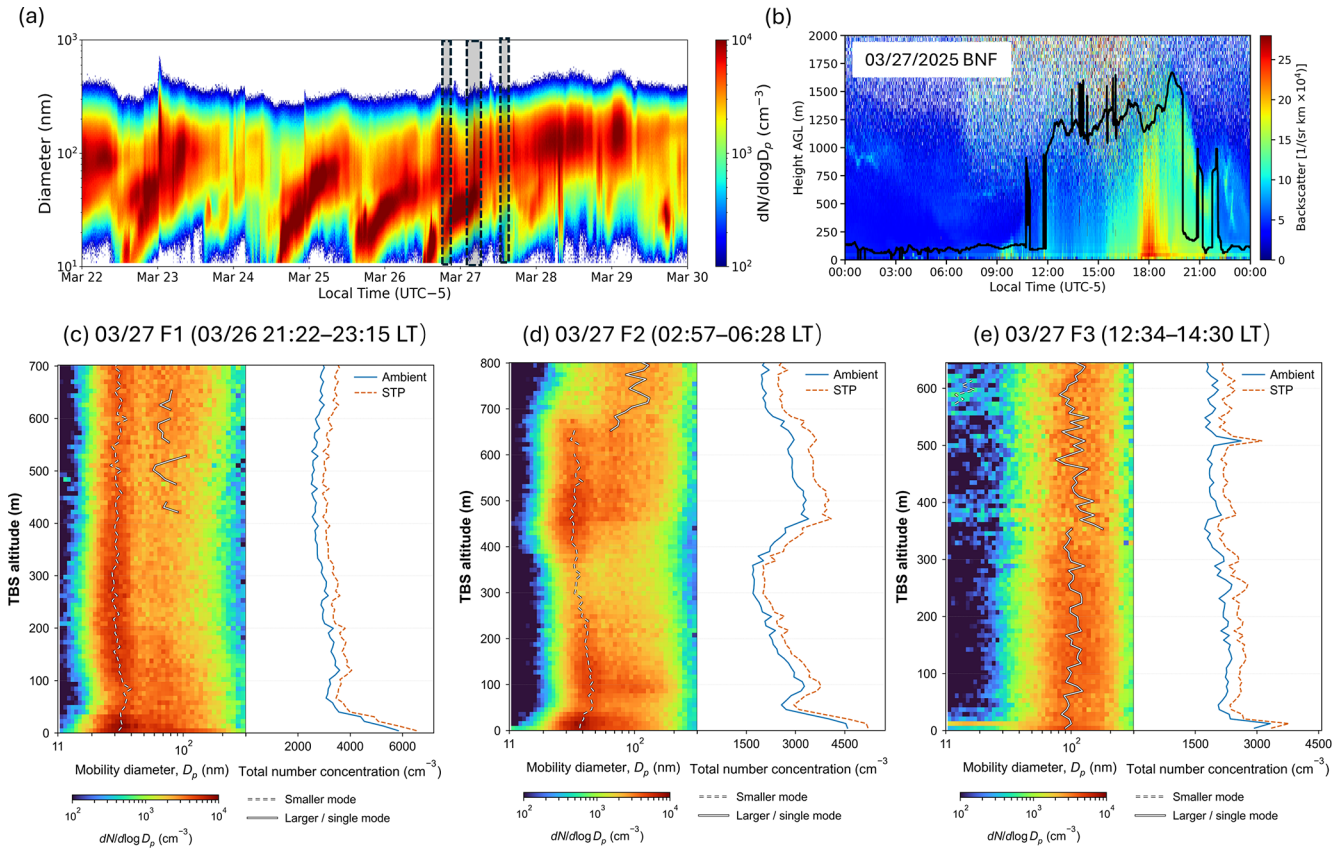

Figure 7. **(a)** Aerosol number size distributions measured by the surface SMPS at the BNF main site from 22–29 March 2025 (the dashed boxes indicate the TBS measurement periods in panels **c**, **d**, and **e**). **(b)** Ceilometer-derived boundary-layer structure and layer heights (black line) at the BNF main site on 27 March 2025 Vertical aerosol size distributions measured by the TBS-mounted mSEMS during **(c)** Flight 1 (26 March 21:22–23:15 LT), **(d)** Flight 2 (02:57–06:28 LT), and **(e)** Flight 3 (12:34–14:30 LT) on 27 March 2025.

ticles larger than 50 nm exhibited little vertical variability. The close agreement in aerosol size distributions between the near-surface layer and the overlying residual layer indicates that the aerosol population remained largely continuous following the collapse of the daytime mixed layer. These observations suggest that particles formed and grown during the previous afternoon's NPF event were well preserved overnight within the residual layer, with only limited modification occurring near the top of the shallow stable boundary layer. The observed reduction in ultrafine particles accompanied by a modest enhancement of accumulation-mode particles is potentially associated with weak turbulent mixing and particle coagulation within this transition layer, although the available observations do not allow these mechanisms to be distinguished and further investigation are warrantied.

By the 27 March F2 flight during 02:57-06:28 LT (Fig. 7d), the aerosol structure had become more heterogeneous than during F1. Within the shallow near-surface layer below 100–150 m, particle populations shifted toward slightly larger diameters, with enhanced concentrations extending into the 50–100 nm size range and a corresponding reduction in particles smaller than 30 nm. This evolution was consistent with the concurrent surface SMPS measurements (Fig. 7a), indicating that aerosol aging within the shallow developing surface layer was not confined to the immediate surface but extended throughout the lower boundary layer. Above the shallow surface layer, particle concentrations decreased markedly between 150 and 400 m, forming a distinct transition layer. Doppler lidar wind profiles obtained during the same period indicated that this altitude range broadly coincided with a transition in the wind field separating the shallow surface layer from a dynamically distinct layer aloft (Fig. S8), suggesting incomplete vertical coupling during the early stages of daytime boundary-layer development. Above 400 m, a relatively stable residual aerosol layer persisted up to about 700 m. Within this layer, the aerosol size distributions remained remarkably similar to those observed during F1, with the persistent 30–50 nm mode largely preserved and particle concentrations slightly enhanced. The close agreement between the two flights indicates that particles formed and grown during the previous day's NPF event remained well preserved within the weakly mixed residual layer, while the developing surface layer had only begun to modify aerosol properties below. Above approximately

700 m, particle modal diameters became slightly larger, coinciding with changes in the wind profile and indicating increasing vertical variability toward the upper portion of the residual layer. Overall, F2 represents an intermediate stage of boundary-layer evolution, characterized by a shallow developing surface layer, a transition layer between approximately 150 and 400 m, and a relatively undisturbed residual-layer core above.

During the 27 March F3 deployment (12:34–14:30 LT, Fig. 7e), the layered aerosol structure had largely disappeared and aerosol size distributions became nearly homogeneous throughout the sampled atmosphere. Concurrent ceilometer observations indicated rapid daytime boundary-layer growth, with the mixed-layer height reaching approximately 650 m, encompassing nearly the entire TBS sampling range. The disappearance of the vertical aerosol gradients coincided with the development of the deep mixed layer, indicating efficient entrainment and recoupling of aerosol populations throughout the lower atmosphere. Taken together, these observations depict a complete evolution in which particles formed during the 26 March NPF event were initially preserved within a vertically homogeneous residual layer overnight, became vertically reorganized during the early-morning transition as boundary-layer growth began, and were subsequently remixed throughout the daytime mixed layer. The persistence of the 30–50 nm particle mode throughout the entire evolution further indicates that the observed vertical structures primarily reflected redistribution of pre-existing particles rather than fresh particle formation.

This case study demonstrated that particle growth events can influence aerosol vertical distributions well beyond the period of active formation and growth. Particles produced during regional growth episodes may remain stored within residual layers overnight and subsequently undergo redistribution as the boundary layer evolves on the following day. Such processes are difficult to infer from surface observations alone and highlight the value of size-resolved vertical measurements for characterizing aerosol evolution within the lower troposphere.

4 Conclusions

This study presents one of the first comprehensive datasets of vertically resolved aerosol particle size distributions obtained using a miniature scanning electrical mobility spectrometer (mSEMS) aboard the DOE ARM Tethered Balloon System across contrasting urban/coastal and forested environments. The observations demonstrate that aerosol vertical structure is closely coupled to boundary-layer evolution and can exhibit substantial variability even when surface aerosol measurements appear relatively uniform. Within the planetary boundary layer, aerosol populations ranged from vertically homogeneous distributions associated with efficient turbulent mixing to heterogeneous structures characterized by surface influence or elevated particle layers enriched in Aitken-mode aerosols. Measurements extending above the PBL further resolved distinct aerosol transitions into the lower free troposphere and the nocturnal residual layer, highlighting atmospheric structures that cannot be fully characterized using boundary-layer height or surface observations alone.

These findings also have implications for interpreting new particle formation events observed at the surface. Although the mSEMS did not resolve nucleation-mode particles smaller than 10 nm, the elevated Aitken-mode populations observed in the upper PBL and above the PBL top suggest that downward transport of previously formed and grown particles may contribute to particle enhancements detected at ground level, as illustrated by the 16 August 2025 case (Sect. 3.1.1). Similarly, particles retained in the residual layer overnight, as observed on 27 March 2025 (Sect. 3.3), may be entrained into the developing mixed layer the following morning, potentially influencing the timing and apparent growth of surface particle populations without concurrent local nucleation. The extent of these effects likely depends on the competing timescales of vertical mixing, particle growth, and coagulation losses. While the present measurements cannot quantify these contributions, future vertically resolved measurements extending below 10 nm, combined with simultaneous surface observations, would help distinguish vertically transported particles from those formed locally.

The case studies further demonstrate that boundary-layer evolution strongly regulates the vertical redistribution of aerosol populations. In particular, the 27 March 2025 BNF TBS observations show that particles produced during a regional growth event were preserved overnight within a residual layer, became vertically reorganized during early-morning boundary-layer redevelopment, and were subsequently remixed throughout the daytime mixed layer. Together with Doppler lidar observations, these measurements provide direct observational evidence linking aerosol vertical structure to boundary-layer dynamics and identify nocturnal residual layers as important reservoirs connecting aerosol evolution across consecutive days. These results highlight the important role of boundary-layer processes in controlling the transport, storage, and redistribution of atmospheric particles within the lower troposphere.

The vertically resolved aerosol size-distribution measurements presented here provide substantially more information on aerosol transport and atmospheric processing than can be obtained from surface observations or boundary-layer height alone. The dataset therefore provides valuable observational constraints for evaluating atmospheric chemistry and transport models and demonstrates the importance of routine vertically resolved aerosol measurements for improving our understanding of aerosol life cycles and boundary-layer processes.

Implications for Future TBS Deployments

Future TBS deployments would benefit from continuous multi-day observations that begin in the pre-dawn and early-morning hours, several hours before the onset of new particle formation, and continue through subsequent particle growth. Flights during this period would capture the aerosol populations stored in the nocturnal residual layer before they are entrained into the developing mixed layer, allowing particles carried over from previous days to be distinguished from those formed locally on the same day. Additional flights extending above the evolving boundary-layer top would further improve characterization of aerosol exchange between the mixed layer, residual layer, and lower free troposphere. Extending the measured size range below 10 nm, for example by deploying a 1 nm condensation particle counter developed at Brookhaven National Laboratory (Kuang et al., 2012) on the TBS alongside the mSEMS, would allow the vertical location of the earliest stages of particle formation to be identified directly. Coordinated observations combining tethered-balloon measurements with higher-altitude uncrewed aerial systems and ground-based remote sensing would provide a more complete picture of aerosol transport and mixing throughout the lower troposphere.

Data availability. The TBS mSEMS data in this study are available at ARM Data Discovery portal at https://doi.org/10.5439/3424399 (Zhang et al., 2026b). Other ARM data, including the surface SMPS measurements as well as the ceilometer measurements are publicly available through the ARM Data Discovery portal (https://adc.arm.gov/discovery/, last access: 16 November 2026).

Supplement. The supplement related to this article is available online at https://doi.org/10.5194/acp-26-16501-2026-supplement.

Author contributions. YG preforms the calculation and data analysis. JZ and FQ designed this study. DD and CK executed the measurements. MS, OE, YW, JM, and GL helped to interpret the results and revised the manuscript. YG and JZ wrote the paper with contributions from all coauthors.

Competing interests. At least one of the (co-)authors is a member of the editorial board of *Atmospheric Chemistry and Physics*. The peer-review process was guided by an independent editor, and the authors also have no other competing interests to declare.

Disclaimer. Publisher's note: Copernicus Publications remains neutral with regard to jurisdictional claims made in the text, published maps, institutional affiliations, or any other geographical representation in this paper. The authors bear the ultimate responsibility for providing appropriate place names. Views expressed in the text are those of the authors and do not necessarily reflect the views of the publisher.

Acknowledgements. The data used in this study were obtained from the Atmospheric Radiation Measurement (ARM) User Facility, a U.S. Department of Energy (DOE) Office of Science user facility managed by the Biological and Environmental Research Program. We gratefully acknowledge the ARM TBS operations team and the staff at the AMF1 CoURAGE and AMF3 Bankhead National Forest (BNF) sites for their outstanding logistical, operational, and technical support during the field deployments. We gratefully acknowledge Kenneth James Davis for his leadership of the CoURAGE campaign and the CoURAGE science team for their contributions. The BNF campaign was led by Chongai Kuang, and we thank the broader BNF science team for their contributions to the campaign. Manish Shrivastava was supported by the U.S. Department of Energy (DOE) Office of Science, Office of Biological and Environmental Research through the Atmospheric System Research program. The Pacific Northwest National Laboratory (PNNL) is operated for DOE by Battelle Memorial Institute under Contract DE-AC06-76RL01830. Chongai Kuang and Ogochukwu Enekwizu were supported by the Biological and Environmental Research Program in the DOE Office of Science through the Brookhaven National Laboratory-led Science Focus Area "PASCCALS", under Contract DE-SC0012704 with Brookhaven Science Associates.

Financial support. This research was supported by start-up funding from the University at Albany and by funding from Dr. Fangqun Yu for the purchase of the mSEMS.

Review statement. This paper was edited by Mingyi Wang and reviewed by three anonymous referees.

References

Blaylock, B., Horel, J., and Liston, S.: Cloud Archiving and Data Mining of High Resolution Rapid Refresh Model Output, Comput. Geosci., 109, 43–50, https://doi.org/10.1016/j.cageo.2017.08.005, 2017.

Brechtel mSEMS Model 9404 Instrument Manual, https://www.brechtel.com/wp-content/uploads/2023/08/bmi_model_9404_mSEMS_manual_v1_3.pdf (last access: 16 November 2026), 2022.

Bulatovic, I., Igel, A. L., Leck, C., Heintzenberg, J., Riipinen, I., and Ekman, A. M. L.: The importance of Aitken mode aerosol particles for cloud sustenance in the summertime high Arctic – a simulation study supported by observational data, Atmos. Chem. Phys., 21, 3871–3897, https://doi.org/10.5194/acp-21-3871-2021, 2021.

Canales, M., Lagos, J., Leiva-Guzmán, M. A. and Toro, R.: Atmospheric stratification dynamics of size-segregated urban particulate matter in the mixed layer using a UAV-mounted aerosol spectrometer, Sci. Total Environ., 1008, 180991, https://doi.org/10.1016/j.scitotenv.2025.180991, 2025.

Carlton, A. G., de Gouw, J., Jimenez, J. L., Ambrose, J. L., Attwood, A. R., Brown, S., Baker, K. R., Brock, C., Cohen, R. C., Edgerton, S., and Farkas, C. M.: Synthesis of the southeast atmosphere studies: Investigating fundamental atmospheric chemistry questions, B. Am. Meteorol. Soc., 99, 547–567, https://doi.org/10.1175/BAMS-D-16-0048.1, 2018.

Carnerero, C., Pérez, N., Reche, C., Ealo, M., Titos, G., Lee, H.-K., Eun, H.-R., Park, Y.-H., Dada, L., Paasonen, P., Kerminen, V.-M., Mantilla, E., Escudero, M., Gómez-Moreno, F. J., Alonso-Blanco, E., Coz, E., Saiz-Lopez, A., Temime-Roussel, B., Marchand, N., Beddows, D. C. S., Harrison, R. M., Petäjä, T., Kulmala, M., Ahn, K.-H., Alastuey, A., and Querol, X.: Vertical and horizontal distribution of regional new particle formation events in Madrid, Atmos. Chem. Phys., 18, 16601–16618, https://doi.org/10.5194/acp-18-16601-2018, 2018.

Chen, B., Thompson, S. A., Matthews, B. H., Sharma, M., Li, R., Nowotarski, C. J., Rapp, A. D., and Brooks, S. D.: A new technique to retrieve aerosol vertical profiles using micropulse lidar and ground-based aerosol measurements, Atmos. Meas. Tech., 18, 5841–5859, https://doi.org/10.5194/amt-18-5841-2025, 2025.

Chen, H., Hodshire, A. L., Ortega, J., Greenberg, J., McMurry, P. H., Carlton, A. G., Pierce, J. R., Hanson, D. R., and Smith, J. N.: Vertically resolved concentration and liquid water content of atmospheric nanoparticles at the US DOE Southern Great Plains site, Atmos. Chem. Phys., 18, 311–326, https://doi.org/10.5194/acp-18-311-2018, 2018.

Davis, K., Zaitchik, B., Asa-Awuku, A., Bou-Zeid, E., Baidar, S., Boxe, C., Brewer, W. A., Chiao, S., Damoah, R., DeCarlo, P., and Demoz, B.: Coastal-Urban-Rural Atmospheric Gradient Experiment (CoURAGE) Science Plan, U.S. Department of Energy, Atmospheric Radiation Measurement user facility, Richland, Washington, DOE/SC-ARM-24-016, https://arm.gov/publications/programdocs/DOE-SC-ARM-24-016.pdf (last access: 16 November 2026), 2024,

Dedrick, J. L., Russell, L. M., Sedlacek III, A. J., Kuang, C., Zawadowicz, M. A., and Lubin, D.: Aerosol-Correlated Cloud Activation for Clean Conditions in the Tropical Atlantic Boundary Layer During LASIC, Geophys. Res. Lette., 51, e2023GL105798, https://doi.org/10.1029/2023GL105798, 2024.

Dexheimer, D., Creamean, J., Gaustad, K., Longbottom, C., Cheng, Z., Sammon, J., and Mei, F.: Tethered Balloon System (TBS) Instrument Handbook. U.S. Department of Energy, Atmospheric Radiation Measurement (ARM) User Facility, DOE/SC-ARM-TR-206, https://doi.org/10.2172/1415858, 2026.

Engvall, A.-C., Krejci, R., Ström, J., Treffeisen, R., Scheele, R., Hermansen, O., and Paatero, J.: Changes in aerosol properties during spring-summer period in the Arctic troposphere, Atmos. Chem. Phys., 8, 445–462, https://doi.org/10.5194/acp-8-445-2008, 2008.

Fan, L., Wu, G., Gao, J., Huang, J., and Chen, G.: Vertical distribution characteristics of aerosol particles at Mt. Qomolangma (Everest) using the tethered balloon, Atmos. Environ., 368, 121798, https://doi.org/10.1016/j.atmosenv.2026.121798, 2026.

Fischer, H., Axinte, R., Bozem, H., Crowley, J. N., Ernest, C., Gilge, S., Hafermann, S., Harder, H., Hens, K., Janssen, R. H. H., Königstedt, R., Kubistin, D., Mallik, C., Martinez, M., Novelli, A., Parchatka, U., Plass-Dülmer, C., Pozzer, A., Regelin, E., Reiffs, A., Schmidt, T., Schuladen, J., and Lelieveld, J.: Diurnal variability, photochemical production and loss processes of hydrogen peroxide in the boundary layer over Europe, Atmos. Chem. Phys., 19, 11953–11968, https://doi.org/10.5194/acp-19-11953-2019, 2019.

Heintzenberg, J., Leck, C., and Tunved, P.: Potential source regions and processes of aerosol in the summer Arctic, Atmos. Chem. Phys., 15, 6487–6502, https://doi.org/10.5194/acp-15-6487-2015, 2015.

James, E. P., Alexander, C. R., Dowell, D. C., Weygandt, S. S., Benjamin, S. G., Manikin, G. S., Brown, J. M., Olson, J. B., Hu, M., Smirnova, T. G., Ladwig, T., Kenyon, J. S., and Turner, D. D.: The High-Resolution Rapid Refresh (HRRR): An hourly updating convection-allowing forecast model. Part II: Forecast performance, Weather Forecast., 37, 1397–1417, https://doi.org/10.1175/WAF-D-21-0130.1, 2022.

Jokinen, T., Lehtipalo, K., Thakur, R. C., Ylivinkka, I., Neitola, K., Sarnela, N., Laitinen, T., Kulmala, M., Petäjä, T., and Sipilä, M.: Measurement report: Long-term measurements of aerosol precursor concentrations in the Finnish subarctic boreal forest, Atmos. Chem. Phys., 22, 2237–2254, https://doi.org/10.5194/acp-22-2237-2022, 2022.

June, N. A., Gaudet, B., Zhao, B., Zawadowicz, M. A., Kuang, C., Shilling, J. E., Guagenti, M., China, S., Fast, J. D., and Shrivastava, M.: Roles of precursor availability and secondary organic aerosol in new particle formation at Bankhead National Forest in spring and summer 2025, Environ. Sci.: Atmos., 6, https://doi.org/10.1039/d6ea00062b, 2026.

Kuang, C.: Spring and Fall Vertically Resolved New Particle Formation and Transport Field Campaign Report, U.S. Department of Energy, Atmospheric Radiation Measurement user facility, Richland, Washington, DOE/SC-ARM-23-012, https://arm.gov/publications/programdocs/doe-sc-arm-23-012.pdf (last access: 16 November 2026), 2023.

Kuang, C., Chen, M., McMurry, P. H., and Wang, J.: Modification of Laminar Flow Ultrafine Condensation Particle Counters for the Enhanced Detection of 1 nm Condensation Nuclei, Aerosol Sci. Tech., 46, 309–315, https://doi.org/10.1080/02786826.2011.626815, 2012.

Kuang, C., Giangrande, S., Serbin, S., Elsaesser, G., Gentine, P., Heus, T., Oue, M., Peters, J., Smith, J., Steiner, A., and McComiskey, A.: Science plan for the deployment of the third ARM mobile facility to the Southeastern United States at the Bankhead National Forest, Alabama (AMF3 BNF), U.S. Department of Energy, Atmospheric Radiation Measurement user facility, Richland, Washington, DOE/SC-ARM-23-035, https://www.arm.gov/publications/programdocs/doe-sc-arm-23-035.pdf (last access: 16 November 2026), 2023.

Kuang, C., Giangrande, S. E., Serbin, S. P., Campbell, P., Elsaesser, G. S., Gentine, P., Heus, T., Hickmon, N. L., Oue, M., Peters, J. M., and Raghunathan, G. N.: The US DOE ARM User Facility Establishes a New Site for Studies of Land–Aerosol–Cloud Interactions in the Southeastern United States, B. Am. Meteorol. Soc., 107, 1–8, https://doi.org/10.1175/BAMS-D-25-0072.1, 2026.

Kulmala, M., Petäjä, T., Nieminen, T., Sipilä, M., Manninen, H. E., Lehtipalo, K., Dal Maso, M., Aalto, P. P., Junninen, H., Paasonen, P., and Riipinen, I.: Measurement of the nucleation of atmospheric aerosol particles, Nat. Protoc., 7, 1651–1667, https://doi.org/10.1038/nprot.2012.091, 2012.

Lai, S., Hai, S., Gao, Y., Wang, Y., Sheng, L., Lupascu, A., Ding, A., Nie, W., Qi, X., Huang, X., and Chi, X.: The striking effect of vertical mixing in the planetary boundary layer on new particle formation in the Yangtze River Delta, Sci. Total Environ., 829, 154607, https://doi.org/10.1016/j.scitotenv.2022.154607, 2022.

Lampilahti, J., Leino, K., Manninen, A., Poutanen, P., Franck, A., Peltola, M., Hietala, P., Beck, L., Dada, L., Quéléver, L., Öhrnberg, R., Zhou, Y., Ekblom, M., Vakkari, V., Zilitinkevich, S., Kerminen, V.-M., Petäjä, T., and Kulmala, M.: Aerosol particle formation in the upper residual layer, Atmos. Chem. Phys., 21, 7901–7915, https://doi.org/10.5194/acp-21-7901-2021, 2021.

Lee, P., Tang, Y., Kang, D., McQueen, J., Tsidulko, M., Huang, H. C., Lu, S., Hart, M., Lin, H. M., Yu, S., and DiMego, G.: Impact of consistent boundary layer mixing approaches between NAM and CMAQ, Environ. Fluid Mech., 9, 23–42, https://doi.org/10.1007/s10652-008-9089-0, 2009.

Lin, Y., Takano, Y., Gu, Y., Wang, Y., Zhou, S., Zhang, T., Zhu, K., Wang, J., Zhao, B., and Chen, G.: Characterization of the aerosol vertical distributions and their impacts on warm clouds based on multi-year ARM observations, Sci. Total Environ., 904, 166582, https://doi.org/10.1016/j.scitotenv.2023.166582, 2023.

Ling, Y., Wang, Y., Duan, J., Xie, X., Liu, Y., Peng, Y., Qiao, L., Cheng, T., Lou, S., Wang, H., and Li, X.: Long-term aerosol size distributions and the potential role of volatile organic compounds (VOCs) in new particle formation events in Shanghai, Atmos. Environ., 202, 345–356, https://doi.org/10.1016/j.atmosenv.2019.01.018, 2019.

Liu, X., Zhao, D., Niu, Z., Zhao, G., Ding, D., Chen, Y., and Liu, H.: Aircraft observations of aerosol and BC during the East Asian dust storm event: Vertical profiles, size distribution and mixing state, Atmos. Environ., 327, 120492, https://doi.org/10.1016/j.atmosenv.2024.120492, 2024.

Mei, F.: Miniaturized Scanning Electrical Mobility Sizer (mSEMS) Instrument Handbook–Airborne Version, U.S. Department of Energy, Atmospheric Radiation Measurement user facility, Richland, Washington, DOE/SC-ARM-TR-310, https://www.osti.gov/servlets/purl/2482517 (last access: 16 November 2026), 2024.

Mei, F., Wang, H., Zhu, Z., Zhang, D., Zhang, Q., Fast, J. D., Gustafson Jr., W. I., Li, X. Y., Schmid, B., Niedek, C., and Tomlinson, J.: Bridging new observational capabilities and process-level simulation: Insights into aerosol roles in the Earth system, B. Am. Meteorol. Soc., 105, 709–724, https://doi.org/10.1175/BAMS-D-23-0110.1, 2024.

Mei, F., Zhang, Q., Zhang, D., Fast, J. D., Kulkarni, G., Pekour, M. S., Niedek, C. R., Glienke, S., Silber, I., Schmid, B., Tomlinson, J. M., Mehta, H. S., Mansoura, X., Cheng, Z., Vandergrift, G. W., Lata, N. N., China, S., and Zhu, Z.: Measurement report: Vertically resolved atmospheric properties observed over the Southern Great Plains with the ArcticShark uncrewed aerial system, Atmos. Chem. Phys., 25, 3425–3444, https://doi.org/10.5194/acp-25-3425-2025, 2025.

Mei, F., Wang, J., Silber, I., Lata, N. N., Vandergrift, G. W., Li, J., Chen, B., Brooks, S. D., Jensen, M. P., Deng, M., Zhang, D., Dexheimer, D., Schmid, B., Cheng, Z., and China, S.: Synthesis of the tethered balloon system and other TRACER campaign measurements elucidates aerosol property profiles, Atmos. Chem. Phys., 26, 13885–13908, https://doi.org/10.5194/acp-26-13885-2026, 2026.

Nieminen, T., Kerminen, V.-M., Petäjä, T., Aalto, P. P., Arshinov, M., Asmi, E., Baltensperger, U., Beddows, D. C. S., Beukes, J. P., Collins, D., Ding, A., Harrison, R. M., Henzing, B., Hooda, R., Hu, M., Hõrrak, U., Kivekäs, N., Komsaare, K., Krejci, R., Kristensson, A., Laakso, L., Laaksonen, A., Leaitch, W. R., Lihavainen, H., Mihalopoulos, N., Németh, Z., Nie, W., O'Dowd, C., Salma, I., Sellegri, K., Svenningsson, B., Swietlicki, E., Tunved, P., Ulevicius, V., Vakkari, V., Vana, M., Wiedensohler, A., Wu, Z., Virtanen, A., and Kulmala, M.: Global analysis of continental boundary layer new particle formation based on long-term measurements, Atmos. Chem. Phys., 18, 14737–14756, https://doi.org/10.5194/acp-18-14737-2018, 2018.

O'Donnell, S. E., Akherati, A., He, Y., Hodshire, A. L., Shilling, J. E., Kuang, C., Fast, J. D., Mei, F., Schobesberger, S., Thornton, J. A., and Smith, J. N.: Look up: Probing the vertical profile of new particle formation and growth in the planetary boundary layer with models and observations, J. Geophys. Res.-Atmos., 128, e2022JD037525, https://doi.org/10.1029/2022JD037525, 2023.

Pöhlker, M. L., Zhang, M., Campos Braga, R., Krüger, O. O., Pöschl, U., and Ervens, B.: Aitken mode particles as CCN in aerosol- and updraft-sensitive regimes of cloud droplet formation, Atmos. Chem. Phys., 21, 11723–11740, https://doi.org/10.5194/acp-21-11723-2021, 2021.

Ran, L., Deng, Z., Wu, Y., Li, J., Bai, Z., Lu, Y., Zhuoga, D., and Bian, J.: Measurement report: Vertical profiling of particle size distributions over Lhasa, Tibet – tethered balloon-based in situ measurements and source apportionment, Atmos. Chem. Phys., 22, 6217–6229, https://doi.org/10.5194/acp-22-6217-2022, 2022.

Rosenfeld, D., Andreae, M. O., Asmi, A., Chin, M., de Leeuw, G., Donovan, D. P., Kahn, R., Kinne, S., Kivekäs, N., and Kulmala, M.: Global observations of aerosol-cloud-precipitation-climate interactions, Rev. Geophys., 52, 750–808, https://doi.org/10.1002/2013RG000441, 2014.

Seinfeld, J. H. and Pandis, S. N.: Atmospheric chemistry and physics: from air pollution to climate change, 3rd edn., John Wiley & Sons, 1152 pp., ISBN: 978-1-118-94740-1, https://www.wiley.com/en-us/shop/general-chemistry/atmospheric-chemistry-and-physics-from-air-pollution-to-climate-change-3rd-edition-p-9781118947401 (last access: 16 November 2026), 2016.

Salma, I., Borsós, T., Weidinger, T., Aalto, P., Hussein, T., Dal Maso, M., and Kulmala, M.: Production, growth and properties of ultrafine atmospheric aerosol particles in an urban environment, Atmos. Chem. Phys., 11, 1339–1353, https://doi.org/10.5194/acp-11-1339-2011, 2011.

Shan, Y., Zhu, Y., Sui, H., Zhao, N., Li, H., Wen, L., Chen, T., Qi, Y., Qi, W., Wang, X., and Zhang, Y.: Vertical distribution and regional transport of air pollution over Northeast China: Insights from an intensive aircraft study, Atmos. Environ., 358, 121327, https://doi.org/10.1016/j.atmosenv.2025.121327, 2025.

Virtanen, P., Gommers, R., Oliphant, T. E., Haberland, M., Reddy, T., Cournapeau, D., Burovski, E., Peterson, P., Weckesser, W., Bright, J., and Van Der Walt, S. J.: SciPy 1.0: fundamental algorithms for scientific computing in Python, Nat. Methods, 17, 261–272, https://doi.org/10.1038/s41592-019-0686-2, 2020.

Wang, Y., Bagya Ramesh, C., Giangrande, S. E., Fast, J., Gong, X., Zhang, J., Tolga Odabasi, A., Oliveira, M. V. B., Matthews, A., Mei, F., Shilling, J. E., Tomlinson, J., Wang, D., and Wang,

J.: Examining the vertical heterogeneity of aerosols over the Southern Great Plains, Atmos. Chem. Phys., 23, 15671–15691, https://doi.org/10.5194/acp-23-15671-2023, 2023.

Williamson, C. J., Kupc, A., Axisa, D., Bilsback, K. R., Bui, T., Campuzano-Jost, P., Dollner, M., Froyd, K. D., Hodshire, A. L., Jimenez, J. L., and Kodros, J. K.: A large source of cloud condensation nuclei from new particle formation in the tropics, Nature, 574, 399–403, https://doi.org/10.1038/s41586-019-1638-9, 2019.

Young, L. H. and Keeler, G. J.: Summertime ultrafine particles in urban and industrial air: Aitken and nucleation mode particle events. Aerosol Air Qual. Res., 7, 379–402, https://doi.org/10.4209/aaqr.2007.02.0012, 2007.

Yu, F., Luo, G., and Hallar, A. G.: Vertical profiles and seasonal variations of key parameters controlling particle formation and growth at Storm Peak Laboratory, Aerosol Air Qual. Res., 16, 900–908, https://doi.org/10.4209/aaqr.2015.05.0368, 2016.

Yu, F., Luo, G., Nair, A. A., Schwab, J. J., Sherman, J. P., and Zhang, Y.: Wintertime new particle formation and its contribution to cloud condensation nuclei in the Northeastern United States, Atmos. Chem. Phys., 20, 2591–2601, https://doi.org/10.5194/acp-20-2591-2020, 2020.

Zhang, J., Yu, F., Kuang, C., and Dexheimer, D.: Seasonal/Spatial Vertical New Particle Formation Variation Study (SSVNV) Field Campaign Report, U.S. Department of Energy, Atmospheric Radiation Measurement User Facility, Richland, Washington, DOE/SC-ARM-26-016, https://arm.gov/publications/programdocs/doe-sc-arm-26-016.pdf (last access: 16 November 2026), 2026a.

Zhang, J., Guo, Y., Yu, F., Kuang, C., and Dexheimer, D.: Tethered Balloon Observations of Vertically Resolved Aerosol Size Distributions during the U.S. DOE ARM CoURAGE and BNF Campaigns, ARM Data Discovery [data set], https://doi.org/10.5439/3424399, 2026b.

Zhang, R., Zhang, D., Mei, F., Mehra, M., Cai, J., Yu, H., Rasheeda A., Carillo-Cardenas, G., Hallar, A., Meskhidze, N., and Wang, Y.: Investigating Ultrafine Aerosol Turbulent Fluxes during Atmospheric New Particle Formation Events, Environ. Sci. Technol., 60, 19984–19998, https://doi.org/10.1021/acs.est.6c06924, 2026.

Zhao, B., Shrivastava, M., Donahue, N. M., Gordon, H., Schervish, M., Shilling, J. E., Zaveri, R. A., Wang, J., Andreae, M. O., Zhao, C., and Gaudet, B.: High concentration of ultrafine particles in the Amazon free troposphere produced by organic new particle formation. P. Natl. Acad. Sci. USA, 117, 25344–25351, https://doi.org/10.1073/pnas.2006716117, 2020.

Zhao, Z., Pang, Y., Qi, B., Zhang, C., Yang, M., and Ye, X.: Vertical profiling of PM_1 and $PM_{2.5}$ dynamics: UAV-based observations in seasonal urban atmosphere, Atmosphere, 16, 968, https://doi.org/10.3390/atmos16080968, 2025.